Australas Phys Eng Sci Med (2017) 40:297–303
DOI 10.1007/s13246-017-0532-8

SCIENTIFIC PAPER

Dosimetry in MARS spectral CT: TOPAS Monte Carlo simulations and ion chamber measurements

Gray Lu[1] · Steven Marsh[1] · Jerome Damet[2,3,4] · Pierre Carbonez[2,4] · John Laban[5] · Christopher Bateman[1,4,6] · Anthony Butler[4,6] · Phil Butler[1,6]

Received: 14 May 2016 / Accepted: 5 February 2017 / Published online: 20 February 2017
© Australasian College of Physical Scientists and Engineers in Medicine 2017

Abstract Spectral computed tomography (CT) is an up and coming imaging modality which shows great promise in revealing unique diagnostic information. Because this imaging modality is based on X-ray CT, it is of utmost importance to study the radiation dose aspects of its use. This study reports on the implementation and evaluation of a Monte Carlo simulation tool using TOPAS for estimating dose in a pre-clinical spectral CT scanner known as the MARS scanner. Simulated estimates were compared with measurements from an ionization chamber. For a typical MARS scan, TOPAS estimated for a 30 mm diameter cylindrical phantom a CT dose index (CTDI) of 29.7 mGy; CTDI was measured by ion chamber to within 3% of TOPAS estimates. Although further development is required, our investigation of TOPAS for estimating MARS scan dosimetry has shown its potential for further study of spectral scanning protocols and dose to scanned objects.

Keywords Medipix · Ionization chamber · Spectral computed tomography · Dosimetry · TOPAS · Monte Carlo simulation · MARS

✉ Gray Lu
gsl29@uclive.ac.nz

1 University of Canterbury, Christchurch, New Zealand

2 CERN, Geneva, Switzerland

3 Institute of Radiation Physics, Lausanne University Hospital, Lausanne, Switzerland

4 Department of Radiology, University of Otago, Christchurch, New Zealand

5 National Centre for Radiation Science, Christchurch, New Zealand

6 MARS Bioimaging Ltd, Christchurch, New Zealand

Introduction

Spectral (multi-energy) CT promises improvements in diagnostic capability over conventional (single-energy) CT systems and other imaging modalities through improvement in image quality, reduction of beam hardening artefacts, superior detection and hence use of contrast agents, and improved tissue contrast. MARS Bioimaging Ltd. in Christchurch, New Zealand are in the process of developing a clinical spectral CT system called the MARS scanner. Spectral CT has been implemented at a pre-clinical stage, currently basing development on small animal sized scanners. As the time of writing, the MARS system incorporates the Medipix3RX energy resolving detectors as these offer the ability to distinguish similar density materials through their unique spectral responses [1]. Taking the next step above dual energy CT, Medipix3RX technology allows simultaneous detection with up to eight energy thresholds. This provides the means to realize 'true' spectral imaging [2–4].

The greater capability of spectral CT also offers enhancement in early diagnostic potential for a variety of diseases, and hence better clinical outcomes. Examples of promising applications include atherosclerosis imaging to observe composition of vulnerable plaque and determining its likelihood of rupture; simultaneous imaging of multiple biomarkers or high-Z nanoparticles bound to cancer seeking drugs, biomarkers or antibodies for early cancer detection; imaging molecular response of cancer to drugs through monitoring high-Z particles with high specificity. Studies in these applications have already been conducted on mice [5].

Medical imaging with CT has long been a prominent driver in the rise of radiation exposure to the public [6]. Even for medical imaging, over-exposure is not without

its consequences [7]. Thus users must be ever vigilant in keeping delivered dose 'as low as reasonably achievable' [8], and developers of new modalities should have this at the forefront of considerations [9]. For spectral CT to rise to prominence, it must provide answers to some key questions: What further clinical applications can spectral CT bring? How will they be implemented through scanning protocol? To achieve the diagnostic goals in human scanning, what will be the magnitude and distribution of radiation dose? To take the first step in answering the latter question, the present study sought to evaluate dosimetry on a small animal spectral CT scanner by implementing a Monte Carlo simulation and verifying it through physical measurements. This study also provided an opportunity to apply Monte Carlo code TOPAS—one which has historically been focused on proton radiotherapy applications—in a diagnostic imaging setting.

Materials and methods

The study focuses on the pre-clinical small animal spectral CT scanner (the MARS scanner) shown in Fig. 1. Main features of the gantry interior include a SB-120-350 Source-Ray Inc. X-ray source unit, adjustable collimation and filtration, and a translatable camera unit featuring the CERN (European Organization for Nuclear Research) developed Medipix3RX detector. The source and camera units can be translated in the x and y directions, while the sample bed can shift in x, y, and z directions for full control of sample imaging position.

Measurements of dose within a mouse-scale phantom were carried out using an ion chamber for a standard scan protocol. The scan protocol chosen for this experiment, referred to hereafter as the 'base' protocol, used the parameters indicated in Table 1 marked with 'base'. This protocol is representative of parameters used in protocols recently investigated within the MARS group.

Matching conditions were simulated using the Monte Carlo toolkit TOPAS version 2.0 [10]. TOPAS is a user code layered on top of the Geant4 Simulation Toolkit [11]. Simulation results were output in comma separated variable (CSV) format and analysed using MATLAB.

Measurements with ionization chamber

The ion chamber used was a Xi CT detector (Unfors RaySafe, Billdal, Sweden). This has an active length of 100 mm and auto correction for temperature and pressure, and an expanded uncertainty of measurement (at reference beam RQA9) below 5% [12]. The Unfors measurement system calibration is traceable to PTB (Physikalisch Technische Bundesanstalt), and to NIST (National Institute of Standards and Technology).

Based on methodology in previous work [13], ion chamber measurements were carried out in a 30 mm diameter cylindrical PMMA (Polymethyl methacrylate) phantom shown in Fig. 2. With the connected ion chamber secured inside, the mounted phantom was positioned such that the centre of the ion chamber sensitive region was directly in front of the collimated beam and at the centre of gantry rotation.

Measurements were made for a series of scans with incremental variation to key parameters. A total of 17 scans were done, and the parameters of each are listed in Table 1. For scans in the 'total filtration' series, it was found that high levels of filtration may cause the dose rate to drop below the ion chamber's lower limit threshold of detectability; for these scans the tube current was boosted to 55 μA. Additional filtration was added by incrementally attaching small plates of Aluminium to the front of the X-ray source unit.

The value measured by the ion chamber is the air kerma to the entire sensitive volume. This needs to be corrected for slice thickness to ascertain what the scan dose would be. The following equation was used, which is in essence the $CTDI_{100}$:

Fig. 1 Photograph of the MARS scanner exterior and the interior with the covers open. The spatial axes of the gantry are indicated

Table 1 List of scans required and the parameters for each

Scan series	*Voltage (kVp)*	*Current (μA)*	*Total filtration (mm Al)*	*SOD (mm)*	*ODD (mm)*	*exposure (ms)*	*projections*
Voltage	80	40	3	200	48	130	360
	90	40	3	200	48	130	360
	100	40	3	200	48	130	360
	110	40	3	200	48	130	360
(base)	118	40	3	200	48	130	360
Current	118	30	3	200	48	130	360
	118	35	3	200	48	130	360
(base)	118	40	3	200	48	130	360
	118	45	3	200	48	130	360
(*)	118	55	3	200	48	130	360
Filtration	118	55	1.8	200	48	130	360
(*)	118	55	3	200	48	130	360
	118	55	4.2	200	48	130	360
	118	55	4.8	200	48	130	360
	118	55	5.4	200	48	130	360
Distance	118	40	3	185	48	130	360
	118	40	3	190	48	130	360
	118	40	3	195	48	130	360
(base)	118	40	3	200	48	130	360
	118	40	3	205	48	130	360

The repeats of the base protocol are marked '(base)', and *marks another redundancy

SOD source object distance, *ODD* object detector distance

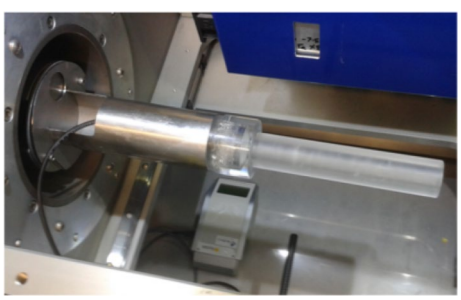

Fig. 2 Ion chamber within PMMA phantom, placed within the gantry of a MARS scanner

$$'CTDI' = M \times \frac{length_{chamber}}{width_{slice}} \quad (1)$$

Here, M is the value of the raw measurement corrected for the chamber active length $length_{chamber}$ and slice thickness $width_{slice}$. The imaged slice width was 11 mm along the z direction.

The scan time for one gantry rotation was measured to be 122 ± 1 s, which includes the 130 ms acquisition time and 360 projections per rotation as well as additional detector processing time. This time is crucial for scaling the Monte Carlo sim1ulation results.

As the values measured with the ion chamber were in terms of air kerma, conversion into absorbed dose to water was required. As a simple conversion, the following equation was used [14]:

$$\frac{K_{col,a}}{K_{col,w}} = \frac{\Psi_a \left(\mu_{en}/\rho\right)_a}{\Psi_w \left(\mu_{en}/\rho\right)_w} \quad (2)$$

In the above equation, K_{col} is the collisional kerma in material, Ψ indicates the photon fluence, $\mu_{en/}\rho$ is the mass energy absorption coefficient, and the subscripts 'w' and 'a' indicates water or air respectively. The conversion requires the following assumptions:

- Negligible radiative loss of energy
- Sufficient build-up is present to ensure charged particle equilibrium
- Radiation energy is sufficiently low that electron path lengths are too short for absorbed dose to exceed kerma at any point, thus $K_{col,w}$ equals absorbed dose to water
- Photon fluence does not change due to the presence of the phantom thus $\Psi_a = \Psi_w$

The ratios of average mass energy absorption coefficients water to air $\left(\overline{\mu}_{en}/\rho\right)_{air}^{w}$ were taken from literature

as a function of half value layer [15]. Relevant HVL values were determined for each kVp and filtration combination using SpekCalc [16]. The HVL values, ranging between 2 and 6 m and depending on beam filtration and kVp, were used to interpolate the tabulated ratios.

Simulation

The Monte Carlo simulation settings generally adopted the TOPAS defaults, except the cut thresholds for photons and electrons were reduced to 0.0001 mm. A variance reduction technique (secondary biasing) was implemented to split photons produced by bremsstrahlung by a factor of 1000, then adjusting for statistical weight. This technique was tested against equivalent 'unbiased' runs to confirm that aside from increased statistical precision per history, the results were not affected.

X-ray source specifications found in the component manual [17] were used to define the source in TOPAS, shown in Fig. 3:

- 1 mm Tungsten target
- 20° anode angle
- 1.8 mm Aluminium equivalent inherent filtration at 120 kVp
- 0.073 mm electron focal spot

As in the MARS scanner, the collimators were defined in the simulation as two pairs of plates, each composed of 3.6 mm thick Lead on a 2 mm thick Aluminium slider. Field size was set by adjusting the position of the collimators. The resulting field size was cross checked with the real field size in the MARS scanner by irradiating Gafchromic film using the chosen scan protocol.

For the electron source, a mono-energetic electron beam of 118 keV with flat spatial distribution and circular cross sectional of 0.0073 mm was used. The electron source, target, filter, and collimators were allocated to a single 'group' which rotated around the origin at 360 angular steps; 250,000 histories were run at each step to simulate the effect of gantry rotation during scanning.

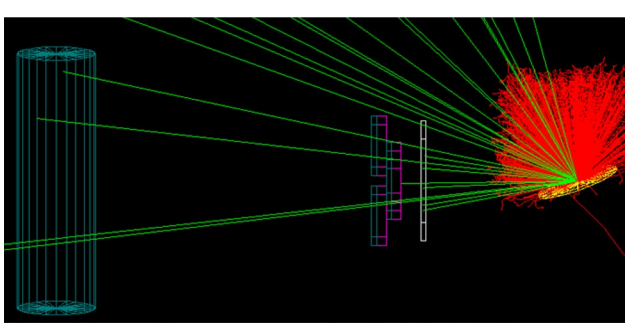

Fig. 3 OpenGL visualisation of TOPAS simulation of X-ray source. Components shown are the anode in *yellow*, the filter in *white*, collimators in *dark green/purple*, photons in *light green*, and electrons in *red*. The cylindrical phantom is also shown in *dark green*

Absorbed dose in Gy (Gray) was scored in a 30 mm diameter water cylinder 100 mm in length, aligned along the z-axis of the gantry and centred at origin. This component was subdivided radially to enable measurement of dose with depth. The dose simulated with Monte Carlo was corrected through the following equation:

$$Dose = \frac{output}{N} \times I \times t \times 6.24 \times 10^{18} \quad (3)$$

Here, the simulation output per number of histories N is scaled to the expected number of X-ray source particles in scan time t and tube current I. The factor 6.24×10^{18} gives the number of electrons in a coulomb. The simulation uncertainty due to random variation was estimated by repeating the base protocol run 5 times with different seeds, then calculating the expanded error (k = 2) from scored doses.

Results

Results for the ion chamber measurements in Fig. 4 show how the measured and converted 'CTDI' is affected by changing each of the 4 key parameters from the base protocol. Also plotted are the results of TOPAS simulation, scored in the water cylinder under equivalent conditions. These simulated values were also corrected for exposed slice thickness using Eq. 1 .

The CTDI value estimated for the base protocol by the simulation was **29.7 ± 0.4** mGy, while the measurement gave **30.3 ± 1.9** mGy.

In Fig. 4a, an increase in CTDI with nominal tube current is shown for both simulation and measurement – showing good agreement. Figure 4b shows an increase in CTDI with nominal tube voltage for both simulation and measurement. There is however, less agreement at tube voltages of 100 kVp or less. Both measured and simulated dose are shown in Fig. 4c to decrease with nominal SOD with good agreement. The effect of filtration on dose shown in Fig. 4d indicate that while dose decreases with added thickness of aluminium, good agreement between measurement and simulation does not extend to minimum filtration.

Discussion

Figure 4 indicates that the dose response to changes in SOD and current are fairly consistent between simulation

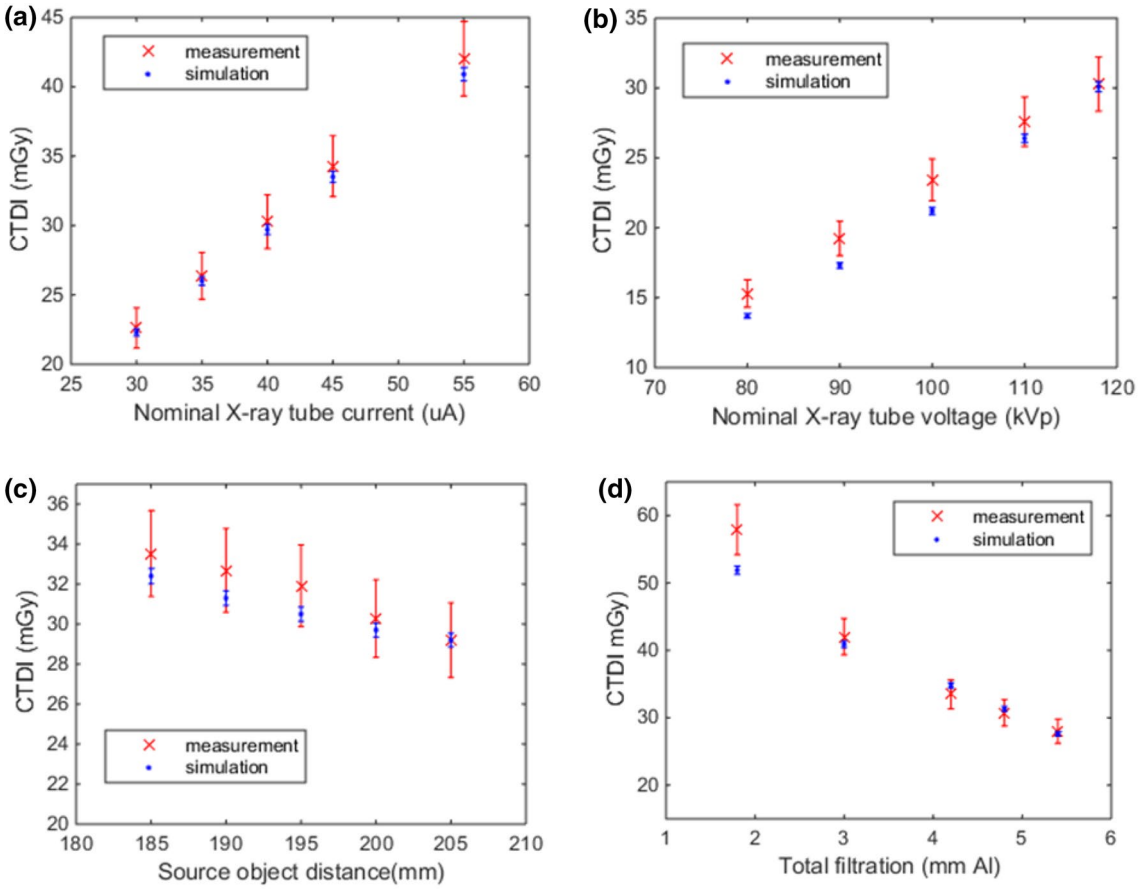

Fig. 4 Plot of CTDI as a function of each key X-ray tube parameter, compared between ion chamber measurement and TOPAS simulation. **a** Tube current. **b** Tube voltage. **c** SOD. **d** Filtration

and measurement, but the response to kVp and filtration changes may not be. The X-ray source manual indicated that inherent filtration can be represented by 1.8 mm Al at 120 kVp. Figure 4b suggests that this may not hold true for kVp much lower than 120 kVp. In reality the inherent filtration due to things like oil coolant or a Beryllium window will likely have a different energy response compared to a solid block of aluminium. Figure 4d similarly implies non-idealities in the X-ray tube output. The effect of additional filtration appears to differ slightly between the simulation and measurements, suggesting there may be differences between the modelled X-ray source and the actual source output; it is also possible that the particle interactions may differ slightly from reality.

Other reasons for deviation may come from the assumptions made in the kerma to dose calculation. The conversion assumes that particle fluence is invariant on whether or not the sensitive volume is air or water, whereas this is likely not the case. Greater fluence in the ion chamber's air cavity compared to water implies the measurements overestimate the dose to a full water phantom. Incidentally we see the majority of measurement points in Fig. 4 are slightly higher than their simulation counterparts. It should also be noted that PMMA is not completely water equivalent. The mass energy absorption coefficient of PMMA begins to differ substantially from water at around <60 keV. This impacts the results as the measurements are made in PMMA while the mass energy absorption ratios used are for water. However this particular factor should only affect the end result by <1% given the magnitude of the corrections themselves.

Uncertainty of the ion chamber measurements was about 5%, but it was found through repeated measurements that X-ray output also varied on average by 4% within a session. It is therefore not unreasonable to assume that there could be even greater variation between different days or time of day, especially considering the effect of room temperature on an air-cooled source. In spite of these relatively large uncertainties, dose is not commonly characterised to the same high accuracy in diagnostic imaging as it is in radiotherapy (which uses much higher doses). This would be especially difficult to achieve on a small scale system using relatively low tube currents and short distances. Any systematic uncertainty would likely have a significant effect on radiation output which may be hard to diagnose with few

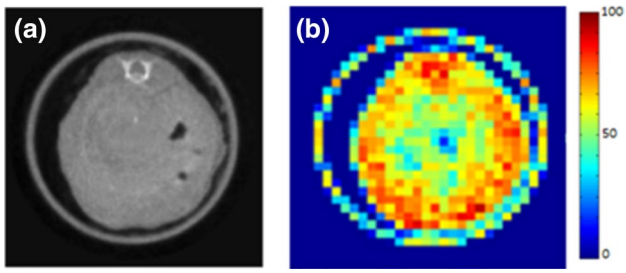

Fig. 5 **a** Transverse CT image of a mouse trunk. **b** Corresponding relative absorbed dose (1 cm *thick*) if irradiated under base protocol conditions, as simulated by TOPAS

data points. However when the technology moves to larger scale imaging, it will be useful to analyse more accurate dose distribution as further exploration of scanning protocol and clinical applications are made.

Monte Carlo tools such as TOPAS offer the capability to spatially map dose in imaged objects. Figure 5 shows image data from a spectral scan imported into TOPAS, resulting in simulation output that can be used to create visualisations of spatial dose distributions. The verification of such estimates and the optimisation of Hounsfield unit to material/electron density conversions in TOPAS for multiple-energy-bin CT data is another area requiring further study. For a start, studies of depth dose in simple objects using dosimeters with high spatial resolution could show the accuracy of TOPAS for calculating dose distribution in 3D. As the development of new spectral CT clinical applications and protocols progress, studying the dose to affected organs in conjunction would better balance diagnostic requirement with the risks associated with dose deposition.

Conclusion

Measurements indicate that for a typical MARS small animal scan, a mouse-sized object will receive an absorbed dose of approximately 30 mGy. A TOPAS based simulation tool has been developed to estimate absorbed dose to scanned samples, and ion chamber measurements have verified these estimates to within 3% (with about 6% uncertainty) for beam energies near 120 kVp. The developed tool is a first step towards the capability to make easy comparisons of future spectral scanning protocols and accurately analysing dose in human scanning. Before advancing onto analysis of spatial dose distribution in such complex scanned objects, the accuracy of TOPAS in calculating spatial dose should be verified with high spatial resolution measurements. This study has also demonstrated the use of TOPAS for diagnostic imaging applications—a break from its traditional application in therapy. Further work has also been identified in simulating dose to objects using spectral image data. With an appropriate image to material assignment it is possible to obtain a 3D dose distribution mapping tool for spectral imaging.

Compliance with ethical standards

Conflict of interest The authors declare that they have no conflict of interest.

Ethical approval This paper does not contain any studies with human participants or animals performed by any of the authors.

References

1. Ballabriga R, Alozy J, Cambell M, Frojdh E, Heijne E, Koenig T, Llopart X, Marchal J, Pennicard D, Poikela T (2016) Review of hybrid pixel detector readout ASICs for spectroscopic X-ray imaging. J Instrum 11:P01007
2. Yu H, Xu Q, He P, Bennett J, Aamir R, Dobbs B, Mou X, Wei B, Butler A, Butler P, Wang G (2012) Medipix-based Spectral Micro-CT. CT Li lun yu ying yong yan jiu 21(4):583
3. Schioppa E, Visser J, Koffeman E (2014) Prospects for spectral CT with Medipix detectors.In: Technology and Instrumentation in Particle Physics 2014, Amsterdam
4. Walsh MF, Nik SJ, Procz S, Pichotka M, De Ruiter N, Chernoglazov AI, RMN. Doesburg, Panta RK, Bell ST, Bateman CJ (2013) Spectral CT data acquisition with Medipix3.1. J Instrum 8:P10012
5. Anderson NG, Butler AP (2014) Clinical applications of spectral molecular imaging: potential and challenges. Contrast Medial Mol Imaging 9:3–12
6. Brenner DJ, Hall EJ (2007) Computed Tomography: an increasing source of radiation exposure. N Engl J Med 357(22):2277–2286
7. Smith-Bindman R (2010) Is Computed Tomography Safe? New Eng J Med 263:1–4
8. International Commission on Radiological Protection (2007) ICRP Publication 103: 2007 Recommendations of the ICRP Elsevier, Amsterdam
9. International Atomic Energy Agency, Wold Health Organisation (2012) Bonn Call for Action In: International conference on radiation protection in medicine: setting the scene for the next decade, IAEA, Bonn
10. Perl J, Shin J, Schumann J, Faddegon B, Paganetti H (2012) TOPAS: An innovative proton Monte Carlo platform for research and clinical applications. Med Phys 39(11):6818–6837
11. Agostinelli S, Allison J, Amako K, Apostolakis J, Araujo H (2003) GEANT4—a simulation toolkit. Nucl Instrum Methods Phys Res 506(3):250–303
12. RaySafe, RaySafe Xi Specifications [Online]. http://mediabank.raysafe.com/A/RaySafe+Media+Bank/1599?encoding=UTF-8. Accessed 4 Dec 2015
13. Ganet N (2015) Dosimetry for spectral molecular imaging of small animals with MARS-CT. In: SPIE. International Society for Optics and Photonics, Orlando

14. Podgorsak EB (2005) Radiation Oncology Physics: A handbook for teachers and students. International Atomic Energy Agency, Vienna
15. Ma CM, Coffey CW, DeWerd LA, Liu C, Nath R, Seltzer SM, Seuntjens JP (2001) AAPM protocol for 40-300kV X-ray beam. Med Phys 26(6):868–893
16. Poludniowski GG, Evans PM (2007) Calculation of X-ray spectra emerging from an X-ray tube. Part I. electron penetration characteristics in X-ray targets. Med Phys 34(6):2164–2174
17. Manez R (2012) Model SB-120-350 (Doc. M-SB120350, Rev 3) Installation/Operation Manual. Source-Ray, Inc., Ronkonkoma